

# UC San Diego

## UC San Diego Previously Published Works

### Title

Carboxylic Acid Isostere Derivatives of Hydroxypyridinones as Core Scaffolds for Influenza Endonuclease Inhibitors

### Permalink

<https://escholarship.org/uc/item/0f00q2ct>

### Journal

ACS Medicinal Chemistry Letters, 14(1)

### ISSN

1948-5875

### Authors

Stokes, Ryjul W  
Kohlbrand, Alysia J  
Seo, Hyeonglim  
[et al.](#)

### Publication Date

2023-01-12

### DOI

10.1021/acsmchemlett.2c00434

Peer reviewed

## Carboxylic Acid Isostere Derivatives of Hydroxypyridinones as Core Scaffolds for Influenza Endonuclease Inhibitors

Ryjul W. Stokes,<sup>‡</sup> Alysia J. Kohlbrand,<sup>‡</sup> Hyeonglim Seo, Banumathi Sankaran, Johannes Karges, and Seth M. Cohen<sup>\*</sup>Cite This: *ACS Med. Chem. Lett.* 2023, 14, 75–82

Read Online

ACCESS |



Metrics &amp; More

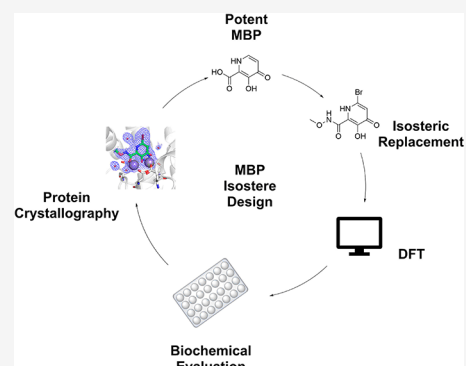


Article Recommendations



Supporting Information

**ABSTRACT:** Among the most important influenza virus targets is the RNA-dependent RNA polymerase acidic N-terminal (PA<sub>N</sub>) endonuclease, which is a critical component of the viral replication machinery. To inhibit the activity of this metalloenzyme, small-molecule inhibitors employ metal-binding pharmacophores (MBPs) that coordinate to the dinuclear Mn<sup>2+</sup> active site. In this study, several metal-binding isosteres (MBIs) were examined where the carboxylic acid moiety of a hydroxypyridinone MBP is replaced with other groups to modulate the physicochemical properties of the compound. MBIs were evaluated for their ability to inhibit PA<sub>N</sub> using a FRET-based enzymatic assay, and their mode of binding in PA<sub>N</sub> was determined using X-ray crystallography.



**KEYWORDS:** drug discovery, metal-binding pharmacophore, isosteres, influenza endonuclease, medicinal inorganic chemistry

Current estimates suggest that annual influenza epidemics are responsible for up to 650,000 deaths globally.<sup>1</sup> One recent study concluded that during the 2009 H1N1 pandemic there were ~61 million cases in the United States alone, resulting in ~275,000 hospitalizations and 12,000 deaths.<sup>2</sup> Vaccines are available; however, efficacy depends on the ability to predict antigenic changes, and requires semi-annual reformulation.<sup>3</sup> To address acute cases of infection, small-molecule therapeutics have been approved by the U.S. Food and Drug Administration (FDA). Adamantane-based structures that inhibited the matrix protein 2 (M2) ion channel have been used,<sup>4</sup> but are now largely not prescribed due to resistance.<sup>5,6</sup> Newer neuraminidase inhibitors are now used,<sup>7</sup> and resistance to neuraminidase inhibitors remains low; however, emergence of resistance remains a threat to public health.<sup>5,8</sup> Other small-molecule strategies to address influenza include targeting the hemagglutinin protein<sup>9</sup> and the RNA-dependent RNA polymerase acidic N-terminal (PA<sub>N</sub>) endonuclease.<sup>10</sup> PA<sub>N</sub> represents an especially attractive target due to its role in viral replication, its high conservation, and its lack of a human analog.<sup>11</sup> FDA approval of baloxavir marboxil, a first-in-class PA<sub>N</sub> inhibitor, has validated this approach,<sup>12</sup> but despite its clinical success, resistance against baloxavir has also begun to emerge.<sup>13</sup>

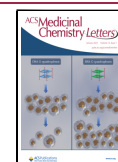
PA<sub>N</sub> is part of a heterotrimeric RNA-dependent RNA polymerase complex, which is composed of PA, PB1, and PB2 subunits.<sup>14</sup> Together, they facilitate replication and transcription of the viral genome.<sup>15</sup> A “cap-snatching” mechanism enables the synthesis of viral mRNA, which can later be

translated into viral proteins.<sup>16</sup> The PA subunit, which enables endonucleolytic cleavage, is composed of a C-terminal domain that is mostly structural and an N-terminal domain that is catalytically active. The N-terminal domain contains a dinuclear Mg<sup>2+</sup> or Mn<sup>2+</sup> active site that is highly conserved.<sup>17–19</sup> Some efforts have used metalloenzyme-focused fragment-based drug discovery (FBDD) to identify potent inhibitors of PA<sub>N</sub>.<sup>20–23</sup> These FBDD campaigns have identified metal-binding pharmacophores (MBPs) that utilize a triad of oxygen donors, including a carboxylic acid, to bind the metal ions, making these fragments very polar and non-ideal starting points for the development of novel therapeutics. To this end, (bio)isosteric replacement is a strategy that can mitigate pharmacological liabilities.<sup>24</sup> Herein, the design and experimental evaluation of novel metal-binding isosteres (MBIs) are reported (Figure 1). The MBIs were found to possess good inhibition of PA<sub>N</sub> endonuclease, with many displaying half-maximal inhibitory concentration (IC<sub>50</sub>) values in the low nanomolar range, comparable to the parent carboxylic acid MBP (compound 1, Figure 1). Using X-ray crystallography, the binding of these compounds to PA<sub>N</sub> was

Received: October 1, 2022

Accepted: December 2, 2022

Published: December 9, 2022



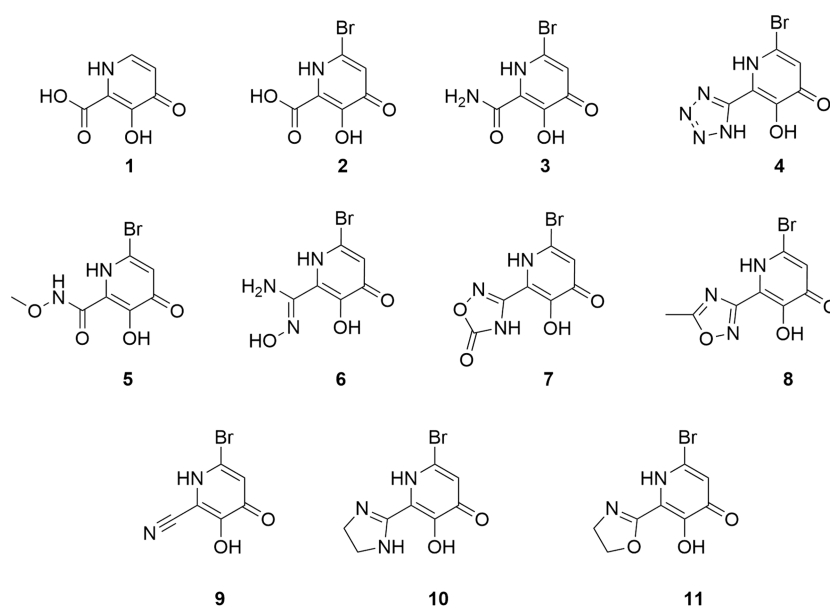


Figure 1. Chemical structures of metal-binding isosteres (MBIs) investigated in this study.

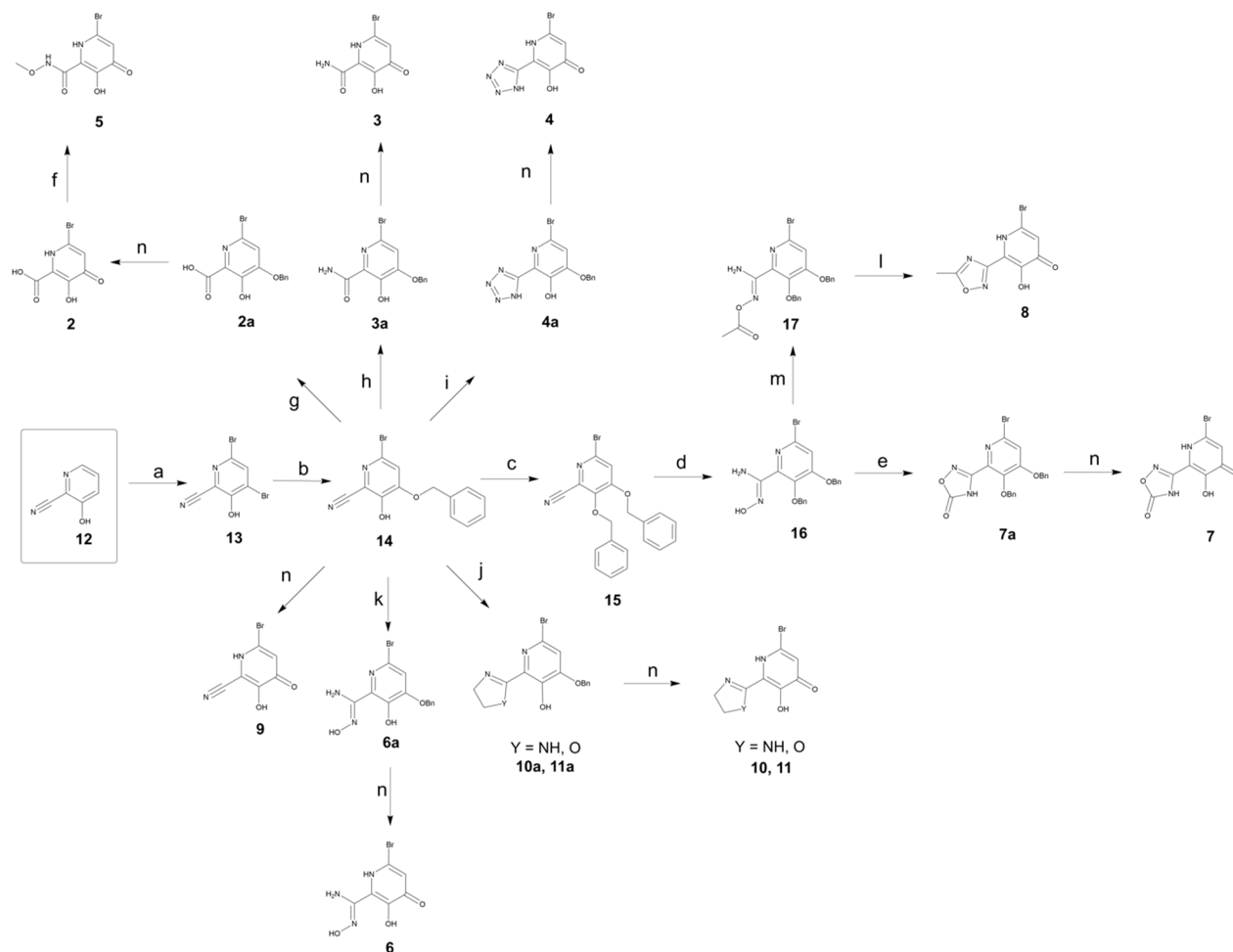
elucidated. While many compounds bound as expected (based on prior findings),<sup>21,22</sup> some isosteres exhibited somewhat unexpected binding interactions. A preliminary analysis of the physical properties, such as calculated log partition coefficient (clogP) and  $pK_a$ , shows that the isosteres have tunable properties, potentially circumventing the limitations of the carboxylic acid scaffold.

Previous work has focused on the identification of MBP fragments and their evolution into lead-like molecules by FBDD.<sup>20–22</sup> A carboxylic acid-modified hydroxypyridinone MBP was reported to achieve  $IC_{50}$  values as low as  $\sim 17$  nM against  $PA_N$ .<sup>21</sup> Hydroxypyridinones have been utilized in drug discovery campaigns, including for their specific ability to coordinate metal ions.<sup>25</sup> Despite impressive activity, this MBP (and elaborated inhibitors derived from it) was found to be only moderately active in influenza-infected cells. This disparity between antiviral activity and enzymatic inhibition is likely due to low membrane permeability originating from the high polarity of these molecules.<sup>19</sup> Additionally, it is well-known that carboxylic acid moieties are associated with pharmacological liabilities, which can limit their use in drug development.<sup>26–28</sup> The carboxylic acid functional group can be replaced by a different moiety with similar biochemical interactions, but different physicochemical properties, via isosteric replacement to try to address possible shortcomings of the carboxylic acid-containing MBP **1** (Figure 1).<sup>24,29</sup>

Nine MBIs (**3–11**) of hydroxypyridinone MBP **1** were synthesized, with isosteric replacements for the carboxylic acid moiety installed (Figure 1). These MBIs also possess a bromine atom in the 6-position of the ring to aid in crystallography (i.e., via heavy-atom substitution and anomalous scattering) and to serve as a synthetic handle for future compound elaboration.<sup>21</sup> To account for the electronic and lipophilic effects of adding this bromine substituent, a direct analog of **1** was synthesized that contains a bromine atom (**2**, Figure 1). Table S1 lists the calculated clogP values of these fragments compared to analogues substituted with -H, -CH<sub>3</sub>, or -Ph groups.

## COMPOUND SYNTHESIS

All bromine-containing compounds (**2–11**) were synthesized from precursor **12**, 3-hydroxypicolinonitrile (Scheme 1). Commercially available **12** can be dibrominated selectively in the 4- and 6-positions upon treatment with elemental bromine to afford **13** in high yield. An oxygen atom that will later participate as a Lewis base to bind the  $Mn^{2+}$  center can be introduced via  $S_NAr$  chemistry. This nucleophilic addition results in the selective introduction of benzyl alcohol in the 4-position to afford intermediate **14** in good yield. Compound **14** serves as a crucial intermediate for the compounds evaluated in this study. Hydrolysis of **14** under basic conditions yields the benzyl-protected compounds **2a** and **3a**, which can be deprotected under acidic conditions to afford compounds **2** and **3**, the acid- and amide-functionalized molecules, respectively. Compound **2** can be further functionalized to incorporate an *N*-methoxycarbonyl group (**5**) by conversion to the acid chloride and subsequent treatment with methoxyamine hydrochloride. A click reaction between compound **14** and sodium azide results in the formation of tetrazole **4a**, a commonly employed carboxylic acid isostere, which can be deprotected to afford the tridentate MBI **4**. Treatment of compound **14** with zinc chloride and ethanolamine or ethylenediamine results in the partially saturated heterocycles **10a** and **11a**. Saturated heterocycles can be advantageous as they tend to have higher lipophilicity, solubility, and three-dimensionality than their unsaturated counterparts.<sup>30</sup> Deprotection of the partially saturated imidazoline (**10**) and oxazoline (**11**). The nitrile group in compound **14** can also be transformed into an *N*-hydroxyamidine functional group when treated with hydroxylamine hydrochloride and triethylamine, followed by debenzoylation to afford compound **6**. Finally, simple deprotection of compound **14** under acidic conditions results in the nitrile-containing MBI **9**. In some cases, protection of the phenol in compound **14** was beneficial. Treatment of **14** with benzyl bromide and potassium carbonate resulted in the formation of **15** in good yield. The protected *N*-hydroxyamide intermediate was synthesized using conditions similar to those used for **6a**, though longer reaction times were

Scheme 1. Synthesis of MBIs<sup>a</sup>

<sup>a</sup>Reagents and conditions: (a) NaOAc, H<sub>2</sub>O:MeOH, Br<sub>2</sub>, 0 °C to 25 °C; (b) NaH, BnOH, DMSO, 60 °C, 18 h; (c) BnBr, K<sub>2</sub>CO<sub>3</sub>, DMF, 45 °C, 19 h; (d) HONH<sub>2</sub>·HCl, NEt<sub>3</sub>, EtOH, 50 °C, 15 h; (e) CDI, NEt<sub>3</sub>, DMF, 80 °C, 8 h; (f) i. SOCl<sub>2</sub>, DCM, reflux, 12 h. ii. Methoxyamine hydrochloride, NEt<sub>3</sub>, DCM, −78 °C to 40 °C, 48 h; (g) NaOH, EtOH, 100 °C, 20 h; (h) KOH, EtOH:H<sub>2</sub>O, 100 °C, 16 h; (i) NaN<sub>3</sub>, NH<sub>4</sub>Cl, DMF, 115 °C, 4 h; (j) ethane-1,2-diamine or 2-aminoethan-1-ol, ZnCl<sub>2</sub>, toluene, 90 °C to 130 °C, 16–20 h; (k) HONH<sub>2</sub>·HCl, NEt<sub>3</sub>, EtOH, 50 °C 1 h; (l) HCl:AcOH:TFA (5:5:1), 50 °C, 48 h; (m) Ac<sub>2</sub>O, DBU, THF, 0 °C to 80 °C, 8 h; (n) HCl, 25 °C to 100 °C, 12–48 h.

employed. Compound **16** can be acylated upon the addition of acetic anhydride to afford compound **17**, which when exposed to heat and a mixture of hydrochloric acid, acetic acid, and trifluoroacetic acid undergoes both debenzoylation and an acid-promoted cyclization to afford oxadiazole **8** in a single step. Additionally, treatment of compound **16** with carbonyldiimidazole (CDI) results in the formation of the oxadiazolone-functionalized molecule **7a**, which can be deprotected to afford compound **7**.

Previous studies have correlated the acidity of the phenolic proton ( $pK_a$ ) of the hydroxypyridinone fragment with the ability to inhibit the activity of PA<sub>N</sub>.<sup>22</sup> In addition, changes in  $pK_a$  can be telling indicators of changes in the electronic structure of the heterocycle. Accordingly,  $pK_a$  values of the MBIs were calculated to probe the electronic differences introduced by the isostere groups. The  $pK_a$  value of the phenolic proton was estimated using density functional theory (DFT) calculations. More precisely, the energetic states within a thermodynamic cycle of the proton-transfer reaction were calculated, and the resulting free energy was correlated to the  $pK_a$  values as has been previously described (see [Supporting Information](#) for details).<sup>31</sup> Compound **2** was predicted to have

a  $pK_a$  value of 9.4. Using a pH-metric titration, the measured  $pK_a$  value of compound **2** was measured at  $9.79 \pm 0.01$ , showing reasonable agreement with the DFT calculation. The isosteric replacement of this functional group was identified as an influencing factor of the acidity of the phenolic proton (a full list of predicted and several additional measured  $pK_a$  values is provided in [Table S2](#)). The isostere modification of the carbonyl group gave calculated  $pK_a$  values ranging from 8.1 to 12.6 ([Table S2](#)), indicating that changes in the 2-position of the hydroxypyridinone ring can have large effects on the electronics of the ring system, and is a useful means to tune the electronic properties of the ring.

To determine the binding mode of the MBIs in the PA<sub>N</sub> active site, several compounds were crystallized with the enzyme for structure determination. Tables of collection and refinement statistics are provided in the [Supporting Information](#) (Tables S3, S4). In native PA<sub>N</sub>, the Mn<sup>2+</sup> cations are coordinated by His41, Glu80, Asp108, Glu 119, and Ile120 and five water molecules, producing an octahedral coordination geometry at each metal center. As anticipated, the addition of a bromine atom to the MBIs produced no apparent change in the binding to the active site metal ions (compare structures of

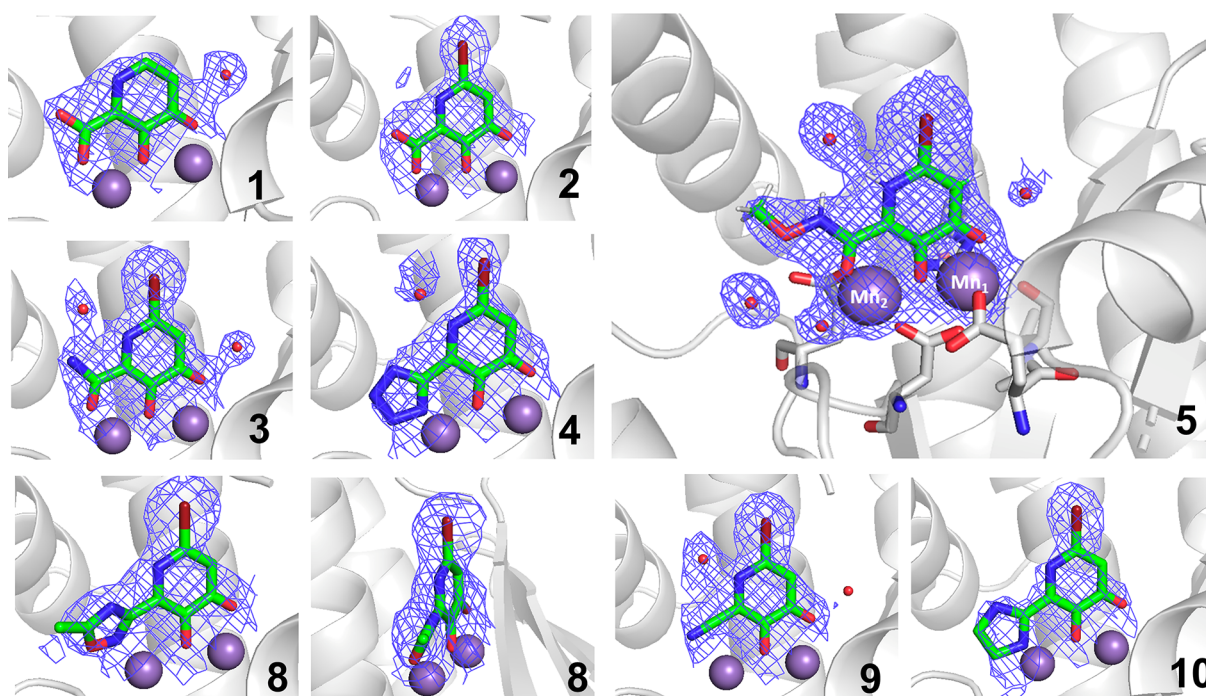


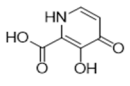
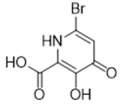
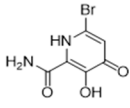
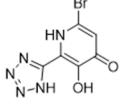
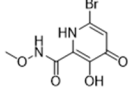
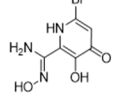
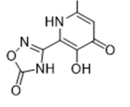
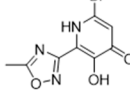
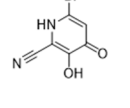
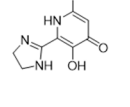
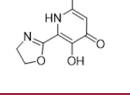
**Figure 2.** Co-crystal structures of PAN endonuclease with compounds 1–5 and 8–10. The large panel depicts MBI 5 coordinating Mn<sub>1</sub> through the exocyclic carbonyl oxygen atom, Mn<sub>2</sub> through the carboxylate group, and the hydroxyl donor bridging between Mn<sub>1</sub> and Mn<sub>2</sub>. The protein backbone is shown as a gray cartoon. Mn<sup>2+</sup> ions and water molecules are shown as purple and red spheres, respectively. The structure with compound 8 is shown from two perspectives. Residues coordinating the Mn<sup>2+</sup> ions are shown in sticks. Atom colors are as follow: carbon (green MBI, gray protein), oxygen (red), nitrogen (blue), bromine (dark red). The electron density of each MBI and the Mn<sup>2+</sup> ions is displayed as a blue mesh. Mesh is  $2F_o - F_c$  contoured at  $2\sigma$ .

1 and 2, Figure 2) and aided in ligand placement within the electron density map. Both compounds 1 and 2 coordinated by bridging the metal ions through the phenolate donor. This provides a triad of oxygen donor atoms (including oxygen donor atoms from the ketone and carboxylic acid groups), creating a 5-membered chelate ring at Mn<sub>1</sub> and a 6-membered chelate ring at Mn<sub>2</sub>. Compounds 1 and 2 also displayed hydrogen bonding between the ketone donor from the hydroxypyridinone ring and Lys134.<sup>32</sup>

Previous crystallographic studies have focused on compounds containing a triad of chelating oxygen atoms that bind in a tridentate fashion, displacing three of the coordinating water molecules.<sup>21,22</sup> Compounds 1, 2, 3, and 5 present the same triad and display similar binding poses, coordinating Mn<sub>1</sub> through the ketone and Mn<sub>2</sub> through the carboxylate, with the hydroxyl group bridging Mn<sub>1</sub> and Mn<sub>2</sub> (Figure 2).<sup>21</sup> The binding and inhibitory activity (vide infra) of these compounds are comparable to those of the parent MBP 1. The average distance from Mn<sub>2</sub> to the carboxylic acid isosteric group in each of these structures is 2.2 Å. A list of metal–donor atom distances is provided in Table S5. Interestingly, several nitrogen-containing isosteres were found to have a bridging water molecule between the nitrogen of the hydroxypyridinone core and a nitrogen from the isosteric groups (see compounds 3, 4, 5, and 9, Figure 2). This interaction is reminiscent of the carbamoylpyridine bicycle in Baloxavir,<sup>19</sup> but creates a cyclized, rigid structure by hydrogen bonding with water, rather than a synthetic, covalent ring structure. This pseudo-five-membered ring may be a useful in future inhibitor design, as it provides conformational stabilization without the necessity to form a bicycle, affording additional synthetic opportunities to develop interactions in the pocket toward Tyr24 and  $\alpha$ -helix 2.

Among structures, compounds 4, 8, 9, and 10 break with the chelating oxygen triad motif by replacing the carboxylic acid oxygen with a nitrogen atom. As expected, Mn<sub>1</sub> is bound between the phenol and the ketone of the hydroxypyridinone core, but unlike previous MBIs with a third oxygen donor, rotations of varying degrees were observed with the heterocyclic MBIs when bound to Mn<sub>2</sub>. Interestingly, the oxadiazolone ring of compound 8 is noticeably rotated out of the plane of the hydroxypyridinone core. A possible explanation for the rotation is the driving force to maintain an octahedral coordination geometry at both metal centers. To preserve an acceptable angle/distance between the metal and the donor atom at both metal sites, a rotation of the heterocyclic isostere may occur, the metal–ligand distances may be adjusted, or a combination thereof. To further examine this hypothesis, octahedral distortion parameters  $\zeta$  and  $\Sigma$  were calculated for compound 8 (relative to Mn<sub>2</sub>) and compared with the distortion parameters of compound 3 and the ligand-free structure, which presented the most ideal octahedral geometries. To calculate and visualize changes in octahedral geometry, Octadist,<sup>33</sup> an octahedral distortion analysis software, was used (Figure S1, Table S6). The  $\zeta$  and  $\Sigma$  values are general octahedral distortion parameters used to characterize deviations from ideal octahedral geometry and are used here to evaluate the isostere binding geometry to Mn<sub>2</sub>.<sup>33</sup> The value of  $\zeta$  is the average of the sum of the deviation of 6 unique metal–ligand bond lengths around the central metal atom ( $d_i$ ) from the average value ( $d_{\text{mean}}$ ).<sup>34</sup> The value of  $\Sigma$  is the sum of the deviation of 12 unique *cis* ligand–metal–ligand angles ( $\phi_i$ ) from 90°.<sup>35,36</sup> These distortion values were calculated for compound 8, although it should be noted that these values do not take into account the resolution of the crystal structure,

**Table 1. Half-Maximal Inhibitory Concentration (IC<sub>50</sub>), 95% Confidence Interval (95% CI), log IC<sub>50</sub> (pIC<sub>50</sub>), and Ligand Efficiency (LE) of Compounds 1–11 against PA<sub>N</sub> Endonuclease**

Compound	Structure	IC <sub>50</sub> (μM)	95% CI	pIC <sub>50</sub>	LE
1		0.05	±0.02	7.30	0.93
2		0.07	±0.04	7.15	0.83
3		0.09	±0.05	7.05	0.82
4		0.09	±0.11	7.05	0.70
5		0.32	±0.02	6.49	0.65
6		0.50	±0.16	6.30	0.68
7		0.04	±0.02	7.40	0.69
8		0.12	±0.06	6.91	0.65
9		0.40	±0.24	6.40	0.81
10		>0.5	-	<6.30	<0.63
11		>0.5	-	<6.30	<0.63

and should be considered accordingly. The value for  $\zeta$  is very small, 0.574 Å, suggesting only very small changes to ligand–metal distances for each of the six donor atoms. The  $\Sigma$  value is also rather small, 90.81°, with the largest deviations from 90° resultant from contributions of the more rigid angles associated with Glu80 and Asp108. When these distortion parameters are

calculated for a structure of compound 8 that is forced into an idealized co-planar ligand geometry, the  $\zeta$  value increases to 0.606 Å and  $\Sigma$  increases to 98.347°, suggesting that the planar MBI structure enforces an inferior octahedral geometry at the metal centers compared to the experimental structure. Comparing both the rotated and planar structures of

compound **8** to those of compound **3** (0.357 Å, 46.669°) and the ligand-free structure (bound water, 0.685 Å, 44.571°), both conformations of compound **8** exhibit poorer octahedral character.

The tetrazole in compound **4** displays a slight twist, perhaps due to the same reason as compound **8**, though the rotation appears less pronounced. Interestingly, instead of incorporating a more distinct twist, this structure adopts different metal–ligand binding distances. The distance between Mn<sub>1</sub> and the ketone functional group is 2.3 Å, while the distance between the tetrazole and Mn<sub>2</sub> is 1.8 Å, both the longest and shortest metal–donor distances observed among these inhibitors, respectively. The average distance from the metal cation in each nitrogen-donating structure is 2.2 Å, matching the donor–metal distance in oxygen triad MBIs, furthering the argument that the rotations of compounds **4** and **8** result from attempting to optimize metal-binding interactions.

Overall, MBIs following the same donor oxygen triad displayed metal-binding activity and binding poses similar to those of previously reported structures. MBIs presenting a nitrogen donor atom instead of the carboxylate oxygen have more variability in metal-binding behavior and pose. Heterocyclic nitrogen MBIs were found to have varying degrees of internal ligand rotation, most notably with compound **8**, which is most likely explained by the need to optimize the octahedral coordination geometry at the Mn<sub>2</sub> metal center.

To determine the activity of these molecules against PA<sub>N</sub>, MBIs were evaluated using a fluorescence-quenching-based nuclease activity assay (see [Supporting Information](#) for details).<sup>37</sup> Using this assay, dose–response curves were obtained to determine the half-maximal inhibitory concentration (IC<sub>50</sub>) values of these compounds. Importantly, IC<sub>50</sub> values are strongly dependent on the buffer, pH, enzyme concentration, and substrate used, and as such may vary somewhat with assay conditions.<sup>38</sup> Here, a protein concentration of 25 nM was employed.<sup>17</sup> As previously identified hydroxypyridinones have been shown to be tight binders of PA<sub>N</sub>,<sup>21</sup> it is expected that molecules with good metal-binding motifs will demonstrate low IC<sub>50</sub> values under these assay conditions.<sup>39</sup> The results of the dose–response experiment are shown in [Table 1](#).

Compound **2** was used as a control to determine whether the addition of a bromine atom negatively affected the metal-binding ability of the MBP. Compounds **1** and **2** showed similar inhibition activity ([Table 1](#)), indicating that the bromide did not impact metal-binding relative to the parent compound. Both compounds display high binding energy per atom (ligand efficiency, LE) ([Table 1](#)). Despite conversion from a potentially anionic carboxylate to a neutral carboxamide, compound **3** showed little difference in activity when compared with compounds **1** or **2**. Compound **4** showed activity comparable to that of the parent structure, possibly due to shorter metal–ligand bond distances ([Table S5](#)). This is perhaps unsurprising, as tetrazoles have been widely investigated as isosteres for carboxylic acids.<sup>40</sup> Compound **5** demonstrated moderate inhibition, suggesting somewhat poorer metal-binding ability, perhaps due to the electron-withdrawing nature of the methoxy group. Compound **7** demonstrated the most potent IC<sub>50</sub> value of the evaluated compounds; however, a crystal structure was not obtained. Compound **8**, functionalized with a methyl-oxadiazole, showed good inhibition, indicating that the rotation of the heterocycle

may contribute to improved metal-binding via optimizing the metal–ligand geometry. While compound **8** does bind favorably, it demonstrates higher distortion parameters than compound **3**, possibly accounting for the decreased activity of **8** compared to **3**. Compound **9** showed relatively poor inhibition, due to the loss of a strong interaction with Mn<sub>2</sub>, which cannot be provided by the nitrile isostere in this context. Previous structures have shown bidentate hydroxypyridinones coordinating to Mn<sub>1</sub>, with the ketone bridging the Mn<sub>1</sub> and Mn<sub>2</sub> metals with the hydroxyl group bound to only Mn<sub>1</sub>.<sup>17,21</sup> Consistent with every structure reported in this study, compound **9** bridges the metal ions through the anionic phenolic group, while the ketone group interacts with Mn<sub>2</sub> and Lys134. This result indicates that even with poorer-binding isosteres like **9**, the introduction of a substituent in the 2-position of the hydroxypyridine ring drives the MBI to coordinate in such a way that bridges the metals with the phenolic group, which is a stronger donor than the ketone and should give better overall affinity. Finally, the saturated heterocycle isosteres **10** and **11** showed markedly poorer inhibition than the parent MBI, possibly due to the softer nature of the heterocyclic donor nitrogen atoms, resulting in poorer electron donation to Mn<sub>2</sub>.

In summary, MBIs of the highly active hydroxypyridinone scaffold were designed to replace the carboxylic acid group and retain inhibition of PA<sub>N</sub> endonuclease. A variety of fragments with isosteric replacements were synthesized via a common intermediate and evaluated in a FRET-based enzymatic assay. Many of these molecules retain inhibitory activity comparable to that of the parent carboxylic acid fragment. These molecules were further evaluated crystallographically to improve our understanding of how the structural and metal-binding properties are affected by replacement of the carboxylic acid group. This study shows that MBIs may be useful in the development of small-molecule therapeutics of influenza PA<sub>N</sub> and other related nucleic-acid-processing viral metalloenzymes.<sup>41,42</sup>

## ■ ASSOCIATED CONTENT

### Supporting Information

The Supporting Information is available free of charge at <https://pubs.acs.org/doi/10.1021/acsmmedchemlett.2c00434>.

Computational prediction of pK<sub>a</sub>, comparative predictions of clogP, predicted phenolic pK<sub>a</sub> values, protein expression and purification, protein crystallography; protein crystallography tables, metal-binding distances, octahedral distortion parameters, octahedral distortion, representative HPLC traces, and lipophilic ligand efficiencies (LLE) ([PDF](#))

SMILES strings formula ([CSV](#))

## ■ AUTHOR INFORMATION

### Corresponding Author

Seth M. Cohen – Department of Chemistry and Biochemistry, University of California, La Jolla, California 92093, United States; [orcid.org/0000-0002-5233-2280](https://orcid.org/0000-0002-5233-2280); Email: [scohen@ucsd.edu](mailto:scohen@ucsd.edu)

### Authors

Ryjul W. Stokes – Department of Chemistry and Biochemistry, University of California, La Jolla, California 92093, United States; [orcid.org/0000-0001-5965-5421](https://orcid.org/0000-0001-5965-5421)

Alysia J. Kohlbrand – Department of Chemistry and Biochemistry, University of California, La Jolla, California 92093, United States

Hyeonlim Seo – Department of Chemistry and Biochemistry, University of California, La Jolla, California 92093, United States

Banumathi Sankaran – The Berkeley Center for Structural Biology, Advanced Light Source, Lawrence Berkeley National Laboratory, Berkeley, California 94720, United States

Johannes Karges – Department of Chemistry and Biochemistry, University of California, La Jolla, California 92093, United States; [orcid.org/0000-0001-5258-0260](https://orcid.org/0000-0001-5258-0260)

Complete contact information is available at:

<https://pubs.acs.org/10.1021/acsmchemlett.2c00434>

### Author Contributions

<sup>‡</sup>R.W.S. and A.J.K. contributed equally to this work.

### Notes

The authors declare the following competing financial interest(s): S.M.C. is a co-founder, has an equity interest, and receives income as member of the Scientific Advisory Board for Forge Therapeutics; is a co-founder, has an equity interest, and is a member of the Scientific Advisory Board for Blacksmith Medicines; and is a co-founder and has an equity interest Cleave Therapeutics (formerly Cleave Biosciences). These companies may potentially benefit from the research results of certain projects in the laboratory of S.M.C. The terms of this arrangement have been reviewed and approved by the University of California, San Diego in accordance with its conflict of interest policies.

### ACKNOWLEDGMENTS

This work was supported by grants from the National Institutes of Health (R01 AI149444) and a National Science Foundation Graduate Research Fellowship Program (DGE-1650112 to R.W.S.). The computational studies were supported in part by the W. M. Keck Foundation through computing resources at the W. M. Keck Laboratory for Integrated Biology. The work used beamlines 5.0.3 and 8.2.1 of the Advanced Light Source, a U.S. DOE Office of Science User Facility, supported in part under Contract No. DE-AC02-05CH11231, and is supported in part by the ALS-ENABLE program funded by the National Institutes of Health, National Institute of General Medical Sciences, Grant P30 GM124169-01. The authors acknowledge Yongxuan Su (U.C. San Diego, Molecular Mass Spectrometry Facility) for aid with MS and HR-MS analysis. The authors also acknowledge Dr. Carlo Ballatore, Bobby Lucero, and Karol Francisco for aid with pK<sub>a</sub> determination and preparatory HPLC.

### ABBREVIATIONS

clogP, calculated log partition coefficient; CDI, carbon-ylidimidazole; DBU, 1,8-diazabicyclo(5.4.0)undec-7-ene; DCM, dichloromethane; DFT, density functional theory; DMF, dimethylformamide; EtOAc, ethyl acetate; FDA, U.S. Food and Drug Administration; IC<sub>50</sub>, half-maximal inhibitory concentration; HAC, heavy atom count; Hex, hexanes; LE, ligand efficiency; M2, matrix protein 2; MBI, metal-binding isostere; MeOH, methanol; MBP, metal-binding pharmacophore; PAN, N-terminal domain of the RNA-dependent RNA polymerase PA subunit; S<sub>N</sub>Ar, nucleophilic aromatic substitution; SAR, structure–activity relationship

### REFERENCES

- (1) Iuliano, A. D.; Roguski, K. M.; Chang, H. H.; Muscatello, D. J.; Palekar, R.; Tempia, S.; Cohen, C.; Gran, J. M.; Schanzer, D.; Cowling, B. J.; Wu, P.; Kyncl, J.; Ang, L. W.; Park, M.; Redlberger-Fritz, M.; Yu, H.; Espenhain, L.; Krishnan, A.; Emukule, G.; van Asten, L.; Pereira da Silva, S.; Aungkulanon, S.; Buchholz, U.; Widdowson, M.-A.; Bresee, J. S.; Azziz-Baumgartner, E.; Cheng, P.-Y.; Dawood, F.; Foppa, I.; Olsen, S.; Haber, M.; Jeffers, C.; MacIntyre, C. R.; Newall, A. T.; Wood, J. G.; Kundi, M.; Popow-Kraupp, T.; Ahmed, M.; Rahman, M.; Marinho, F.; Sotomayor Proschle, C. V.; Vergara Mallegas, N.; Luzhao, F.; Sa, L.; Barbosa-Ramirez, J.; Sanchez, D. M.; Gomez, L. A.; Vargas, X. B.; Acosta Herrera, A.; Llanes, M. J.; Fischer, T. Køl.; Krause, T. G.; Mølbak, K.; Nielsen, J.; Trebbien, R.; Bruno, A.; Ojeda, J.; Ramos, H.; an der Heiden, M.; del Carmen Castillo Signor, L.; Serrano, C. E.; Bhardwaj, R.; Chadha, M.; Narayan, V.; Kosen, S.; Bromberg, M.; Glatman-Freedman, A.; Kaufman, Z.; Arima, Y.; Oishi, K.; Chaves, S.; Nyawanda, B.; Al-Jarallah, R. A.; Kuri-Morales, P. A.; Matus, C. R.; Corona, M. E. J.; Burmaa, A.; Darmaa, O.; Obtel, M.; Cherkaoui, I.; van den Wijngaard, C. C.; van der Hoek, W.; Baker, M.; Bandaranayake, D.; Bissielo, A.; Huang, S.; Lopez, L.; Newbern, C.; Flem, E.; Grøneng, G. M.; Hauge, S.; de Cosio, F. G.; de Molto, Y.; Castillo, L. M.; Cabello, M. A.; van Horoch, M.; Medina Osis, J.; Machado, A.; Nunes, B.; Rodrigues, A. P.; Rodrigues, E.; Calomfirescu, C.; Lupulescu, E.; Popescu, R.; Popovici, O.; Bogdanovic, D.; Kostic, M.; Lazarevic, K.; Milosevic, Z.; Todorovic, B.; Chen, M.; Cutter, J.; Lee, V.; Lin, R.; Ma, S.; Cohen, A. L.; Treurnicht, F.; Kim, W. J.; Delgado-Sanz, C.; de mateo Ontanon, S.; Larrauri, A.; Leon, I. L.; Vallejo, F.; Born, R.; Junker, C.; Koch, D.; Chuang, J.-H.; Huang, W.-T.; Kuo, H.-W.; Tsai, Y.-C.; Bundhamcharoen, K.; Chittaganpitch, M.; Green, H. K.; Pebody, R.; Goni, N.; Chiparelli, H.; Brammer, L.; Mustaqim, D.; et al. Estimates of global seasonal influenza-associated respiratory mortality: a modelling study. *Lancet* **2018**, *391*, 1285–1300.
- (2) Shrestha, S. S.; Swerdlow, D. L.; Borse, R. H.; Prabhu, V. S.; Finelli, L.; Atkins, C. Y.; Owusu-Edusei, K.; Bell, B.; Mead, P. S.; Biggerstaff, M.; Brammer, L.; Davidson, H.; Jernigan, D.; Jung, M. A.; Kamimoto, L. A.; Merlin, T. L.; Nowell, M.; Redd, S. C.; Reed, C.; Schuchat, A.; Meltzer, M. I. Estimating the Burden of 2009 Pandemic Influenza A (H1N1) in the United States (April 2009–April 2010). *Clin. Infect. Dis.* **2011**, *52*, S75–S82.
- (3) Lewnard, J. A.; Cobey, S. Immune History and Influenza Vaccine Effectiveness. *Vaccines* **2018**, *6*, 28.
- (4) Pielak, R. M.; Chou, J. J. Influenza M2 proton channels. *Biochim. Biophys. Acta, Biomembr.* **2011**, *1808*, 522–529.
- (5) Principi, N.; Camilloni, B.; Alunno, A.; Polinori, I.; Argentiero, A.; Esposito, S. Drugs for Influenza Treatment: Is There Significant News? *Front. Med.* **2019**, *6*, 109.
- (6) Bright, R. A.; Shay, D. K.; Shu, B.; Cox, N. J.; Klimov, A. I. Adamantane Resistance Among Influenza A Viruses Isolated Early During the 2005–2006 Influenza Season in the United States. *JAMA* **2006**, *295*, 891–894.
- (7) Moscona, A. Neuraminidase Inhibitors for Influenza. *N. Engl. J. Med.* **2005**, *353*, 1363–1373.
- (8) Kim, H. M.; Lee, N.; Kim, M.-S.; Kang, C.; Chung, Y.-S. Characterization of neuraminidase inhibitor-resistant influenza virus isolates from immunocompromised patients in the Republic of Korea. *Virology* **2020**, *17*, 94.
- (9) Sriwilajaroen, N.; Suzuki, Y. Molecular basis of the structure and function of H1 hemagglutinin of influenza virus. *Proc. Jpn. Acad., Ser. B* **2012**, *88*, 226–249.
- (10) Yuan, P.; Bartlam, M.; Lou, Z.; Chen, S.; Zhou, J.; He, X.; Lv, Z.; Ge, R.; Li, X.; Deng, T.; Fodor, E.; Rao, Z.; Liu, Y. Crystal structure of an avian influenza polymerase PAN reveals an endonuclease active site. *Nature* **2009**, *458*, 909–913.
- (11) Monod, A.; Swale, C.; Tarus, B.; Tissot, A.; Delmas, B.; Ruigrok, R. W.; Crépin, T.; Slama-Schwok, A. Learning from structure-based drug design and new antivirals targeting the ribonucleoprotein complex for the treatment of influenza. *Expert Opin. Drug Discovery* **2015**, *10*, 345–371.



- (12) Ng, K. E. Xofluza (Baloxavir Marboxil) for the Treatment Of Acute Uncomplicated Influenza. *P&T* **2019**, *44*, 9–11.
- (13) Checkmahomed, L.; M'Hamdi, Z.; Carbonneau, J.; Venable, M. C.; Baz, M.; Abed, Y.; Boivin, G. Impact of the Baloxavir-Resistant Polymerase Acid I38T Substitution on the Fitness of Contemporary Influenza A(H1N1)pdm09 and A(H3N2) Strains. *J. Infect. Dis.* **2020**, *221*, 63–70.
- (14) Resa-Infante, P.; Jorba, N.; Coloma, R.; Ortin, J. The influenza virus RNA synthesis machine: advances in its structure and function. *RNA Biol.* **2011**, *8*, 207–215.
- (15) Hutchinson, E. C.; Fodor, E. Transport of the influenza virus genome from nucleus to nucleus. *Viruses* **2013**, *5*, 2424–2446.
- (16) Dias, A.; Bouvier, D.; Crépin, T.; McCarthy, A. A.; Hart, D. J.; Baudin, F.; Cusack, S.; Ruigrok, R. W. H. The cap-snatching endonuclease of influenza virus polymerase resides in the PA subunit. *Nature* **2009**, *458*, 914–918.
- (17) Bauman, J. D.; Patel, D.; Baker, S. F.; Vijayan, R. S. K.; Xiang, A.; Parhi, A. K.; Martínez-Sobrido, L.; LaVoie, E. J.; Das, K.; Arnold, E. Crystallographic Fragment Screening and Structure-Based Optimization Yields a New Class of Influenza Endonuclease Inhibitors. *ACS Chem. Biol.* **2013**, *8*, 2501–2508.
- (18) Jones, J. C.; Marathe, B. M.; Lerner, C.; Kreis, L.; Gasser, R.; Pascua, P. N. Q.; Najera, I.; Govorkova, E. A. A Novel Endonuclease Inhibitor Exhibits Broad-Spectrum Anti-Influenza Virus Activity In Vitro. *Antimicrob. Agents Chemother.* **2016**, *60*, 5504–5514.
- (19) Miyagawa, M.; Akiyama, T.; Taoda, Y.; Takaya, K.; Takahashi-Kageyama, C.; Tomita, K.; Yasuo, K.; Hattori, K.; Shano, S.; Yoshida, R.; Shishido, T.; Yoshinaga, T.; Sato, A.; Kawai, M. Synthesis and SAR Study of Carbamoyl Pyridone Bicycle Derivatives as Potent Inhibitors of Influenza Cap-dependent Endonuclease. *J. Med. Chem.* **2019**, *62*, 8101–8114.
- (20) Credille, C. V.; Chen, Y.; Cohen, S. M. Fragment-Based Identification of Influenza Endonuclease Inhibitors. *J. Med. Chem.* **2016**, *59*, 6444–6454.
- (21) Credille, C. V.; Morrison, C. N.; Stokes, R. W.; Dick, B. L.; Feng, Y.; Sun, J.; Chen, Y.; Cohen, S. M. SAR Exploration of Tight-Binding Inhibitors of Influenza Virus PA Endonuclease. *J. Med. Chem.* **2019**, *62*, 9438–9449.
- (22) Credille, C. V.; Dick, B. L.; Morrison, C. N.; Stokes, R. W.; Adamek, R. N.; Wu, N. C.; Wilson, I. A.; Cohen, S. M. Structure–Activity Relationships in Metal-Binding Pharmacophores for Influenza Endonuclease. *J. Med. Chem.* **2018**, *61*, 10206–10217.
- (23) Karges, J.; Stokes, R. W.; Cohen, S. M. Photorelease of a metal-binding pharmacophore from a Ru(II) polypyridine complex. *Dalton Trans.* **2021**, *50*, 2757–2765.
- (24) Lassalas, P.; Gay, B.; Lasfargeas, C.; James, M. J.; Tran, V.; Vijayendran, K. G.; Brunden, K. R.; Kozlowski, M. C.; Thomas, C. J.; Smith, A. B.; Huryn, D. M.; Ballatore, C. Structure Property Relationships of Carboxylic Acid Isosteres. *J. Med. Chem.* **2016**, *59*, 3183–3203.
- (25) Santos, M. A.; Marques, S. M.; Chaves, S. Hydroxypyridinones as “privileged” chelating structures for the design of medicinal drugs. *Coord. Chem. Rev.* **2012**, *256* (1), 240–259.
- (26) Lassila, T.; Hokkanen, J.; Aatsinki, S.-M.; Mattila, S.; Turpeinen, M.; Tolonen, A. Toxicity of Carboxylic Acid-Containing Drugs: The Role of Acyl Migration and CoA Conjugation Investigated. *Chem. Res. Toxicol.* **2015**, *28*, 2292–2303.
- (27) Pajouhesh, H.; Lenz, G. R. Medicinal chemical properties of successful central nervous system drugs. *NeuroRx* **2005**, *2*, 541–553.
- (28) Dick, B. L.; Cohen, S. M. Metal-Binding Isosteres as New Scaffolds for Metalloenzyme Inhibitors. *Inorg. Chem.* **2018**, *57*, 9538–9543.
- (29) Patani, G. A.; LaVoie, E. J. Bioisosterism: A Rational Approach in Drug Design. *Chem. Rev.* **1996**, *96*, 3147–3176.
- (30) Marson, C. M. Saturated Heterocycles with Applications in Medicinal Chemistry. In *Advances in Heterocyclic Chemistry*; Scriven, E. F. V., Ramsden, C. A., Eds.; Academic Press: 2017; Vol. 121, Chap. 2, 13–33.
- (31) Pliego, J. R. Thermodynamic cycles and the calculation of pKa. *Chem. Phys. Lett.* **2003**, *367* (1), 145–149.
- (32) Zhang, C.; Xiang, J.; Xie, Q.; Zhao, J.; Zhang, H.; Huang, E.; Shaw, P.; Liu, X.; Hu, C. Identification of Influenza PAN Endonuclease Inhibitors via 3D-QSAR Modeling and Docking-Based Virtual Screening. *Molecules* **2021**, *26*, 7129.
- (33) Ketkaew, R.; Tantirungrotechai, Y.; Harding, P.; Chastanet, G.; Guionneau, P.; Marchivie, M.; Harding, D. J. OctaDist: a tool for calculating distortion parameters in spin crossover and coordination complexes. *Dalton Trans.* **2021**, *50*, 1086–1096.
- (34) Buron-Le Cointe, M.; Hébert, J.; Baldé, C.; Moisan, N.; Toupet, L.; Guionneau, P.; Létard, J. F.; Freysz, E.; Cailleau, H.; Collet, E. Intermolecular control of thermoswitching and photo-switching phenomena in two spin-crossover polymorphs. *Phys. Rev. B* **2012**, *85*, 064114.
- (35) Drew, M. G. B.; Harding, C. J.; McKee, V.; Morgan, G. G.; Nelson, J. Geometric control of manganese redox state. *J. Chem. Soc., Chem. Commun.* **1995**, 1035–1038.
- (36) Guionneau, P.; Brigouleix, C.; Barrans, Y.; Goeta, A. E.; Létard, J.-F.; Howard, J. A. K.; Gaultier, J.; Chasseau, D. High pressure and very low temperature effects on the crystal structures of some iron(II) complexes. *C. R. Acad. Sci., Ser. IIC: Chim.* **2001**, *4*, 161–171.
- (37) Baughman, B. M.; Jake Slavish, P.; DuBois, R. M.; Boyd, V. A.; White, S. W.; Webb, T. R. Identification of Influenza Endonuclease Inhibitors Using a Novel Fluorescence Polarization Assay. *ACS Chem. Biol.* **2012**, *7*, 526–534.
- (38) Kalliokoski, T.; Kramer, C.; Vulpetti, A.; Geddeck, P. Comparability of Mixed IC50 Data – A Statistical Analysis. *PLoS One* **2013**, *8*, e61007.
- (39) Todd, B.; Tchesnokov, E. P.; Götte, M. The active form of the influenza cap-snatching endonuclease inhibitor baloxavir marboxil is a tight binding inhibitor. *J. Biol. Chem.* **2021**, *296*, 100486.
- (40) Malik, M. A.; Wani, M. Y.; Al-Thabaiti, S. A.; Shiekh, R. A. Tetrazoles as carboxylic acid isosteres: chemistry and biology. *J. Inclusion Phenom. Macrocyclic Chem.* **2014**, *78*, 15–37.
- (41) Agrawal, A.; DeSoto, J.; Fullagar, J. L.; Maddali, K.; Rostami, S.; Richman, D. D.; Pommier, Y.; Cohen, S. M. Probing chelation motifs in HIV integrase inhibitors. *Proc. Natl. Acad. Sci. U. S. A.* **2012**, *109*, 2251–2256.
- (42) Šebera, J.; Dubankova, A.; Sychrovský, V.; Ruzek, D.; Boura, E.; Nencka, R. The structural model of Zika virus RNA-dependent RNA polymerase in complex with RNA for rational design of novel nucleotide inhibitors. *Sci. Rep.* **2018**, *8*, 11132.